Cooperative assembly and dynamic disassembly of MDA5 filaments for viral dsRNA recognition

Alys Peisley[a,b], Cecilie Lin[c], Bin Wu[a,b], McGhee Orme-Johnson[a], Mengyuan Liu[d], Thomas Walz[c,e], and Sun Hur[a,b,1]

[a]The Immune Disease Institute, Children's Hospital Boston, Boston, MA 02115; [b]Department of Biological Chemistry and Molecular Pharmacology, Harvard Medical School, Boston, MA 02115; [c]Department of Cell Biology, Harvard Medical School, Boston, MA 02115; [d]Department of Molecular Cellular Biology, Harvard University, Boston, MA 02115; and [e]Howard Hughes Medical Institute, Harvard Medical School, Boston, MA 02115

Edited by John Kuriyan, University of California, Berkeley, CA, and approved October 17, 2011 (received for review August 19, 2011)

MDA5, an RIG-I-like helicase, is a conserved cytoplasmic viral RNA sensor, which recognizes dsRNA from a wide-range of viruses in a length-dependent manner. It has been proposed that MDA5 forms higher-order structures upon viral dsRNA recognition or during antiviral signaling, however the organization and nature of this proposed oligomeric state is unknown. We report here that MDA5 cooperatively assembles into a filamentous oligomer composed of a repeating segmental arrangement of MDA5 dimers along the length of dsRNA. Binding of MDA5 to dsRNA stimulates its ATP hydrolysis activity with little coordination between neighboring molecules within a filament. Individual ATP hydrolysis in turn renders an intrinsic kinetic instability to the MDA5 filament, triggering dissociation of MDA5 from dsRNA at a rate inversely proportional to the filament length. These results suggest a previously unrecognized role of ATP hydrolysis in control of filament assembly and disassembly processes, thereby autoregulating the interaction of MDA5 with dsRNA, and provides a potential basis for dsRNA length-dependent antiviral signaling.

pattern recognition receptor | receptor clustering | dynamic instability

Effective immune defense against viral infection depends on accurate and robust detection of viral RNAs by pattern recognition receptors in the innate immune system. RIG-I and MDA5 are conserved viral RNA receptors in vertebrates, sharing similar domain architectures and approximately 30% sequence identity. They are functional in the cytoplasm and responsible for detection of viral RNAs present during viral infection in a broad range of tissues (1). Upon viral RNA recognition, RIG-I and MDA5 interact with a common signaling adaptor, MAVS and activate NF-kB and IRF3/7 signaling pathways, resulting in the expression of type I interferon and proinflammatory cytokines (2).

Previous studies suggested that RIG-I and MDA5 recognize largely distinct groups of viruses through their divergent RNA specificity (3, 4). RIG-I detects a variety of positive and negative strand viruses through recognition of a 5′ triphosphate group and blunt ends of genomic RNAs (3, 5, 6). By contrast, MDA5 detects several positive strand and dsRNA viruses such as picornaviruses and reoviruses through recognition of dsRNA replication intermediates and genomic dsRNAs (3, 4, 7). This viral RNA recognition by MDA5 is independent of 5′ triphosphate or blunt end, but instead depends on dsRNA length in a range of approximately 1–7 kb (8).

The precise mechanism for length-dependent dsRNA recognition by MDA5 is poorly understood. Previous studies suggest that ATP hydrolysis could play an important role in both interferon signaling and RNA specificity (1, 2). The current model of MDA5 (or RIG-I) mediated signal activation is that binding of viral RNA to MDA5 triggers ATP hydrolysis in the conserved helicase domain, which then alters the receptor conformations or accessibility of the signaling domain (a tandem caspase activation recruitment domain) to allow its interaction with MAVS (1, 9). The proposed role of ATP hydrolysis as a conformational switch for signaling is supported by the requirement of ATP in the reconstituted signaling system of RIG-I (9, 10) and the observation that mutations in the active site for ATP hydrolysis either constitutively activate or inactivate interferon signaling by RIG-I and MDA5 (11, 12). In addition, induction of ATP hydrolysis by dsRNA has been shown to correlate with stimulation of interferon signaling (6, 13).

It has been proposed that MDA5 (and RIG-I) forms a higher-order structure during viral RNA recognition for efficient antiviral signaling (14–16). Receptor oligomerization or clustering, as demonstrated in other receptors, such as inflammasomes, Toll-like receptors, T- and B-cell receptors, is often important for ligand sensitivity and downstream signaling efficiency (17, 18). To understand the assembly architecture of the postulated higher-order structure and a potential role for ATP hydrolysis in structural reorganization, we used a combination of EM, biochemical, and kinetic analyses. We demonstrate here that MDA5 assembles into a filamentous oligomer along the length of dsRNA and dynamically regulates its disassembly process through ATP hydrolysis in a length-dependent manner. This study provides a mechanism of how MDA5 both recognizes dsRNA and autoregulates its antiviral signaling potential in a dsRNA length-dependent manner.

Results

MDA5 Binding to dsRNA is Cooperative. Antiviral signaling through MDA5 is stimulated by dsRNA but not by ssRNA or dsDNA (8, 19). To examine whether the differential binding affinities of MDA5 are responsible for dsRNA specificity, we purified recombinant human MDA5 from *Escherichia coli* (Fig. S1*A*) and examined its interaction with 112 bp dsRNA and dsDNA, and 112 nt ssRNA using an EMSA. These model nucleic acids were derived from MDA5 cDNA (Table S1), and no significant secondary structure was predicted for the ssRNA (mFold).

EMSA revealed that MDA5 is capable of high-affinity binding to dsRNA, dsDNA, and ssRNA with dissociation constants (K_d) of 22, 33, and 57 nM, respectively (Fig. 1). Despite the comparable binding affinities between the nucleic acid types, only the interaction between MDA5 and dsRNA is highly cooperative. By EMSA, MDA5 addition to dsRNA resulted in a bimodal distribution of mostly either free (RNA-only) or saturated (fully complexed) products (Fig. 1*A*). By contrast, MDA5 complexed with ssRNA or dsDNA exhibits a broad distribution of intermediate sizes, indicative of less cooperative binding. In a quantitative analysis of the EMSA results (Fig. 1*B*), the dsRNA binding curve is sharply sigmoidal with a Hill coefficient of 4.0, whereas the binding curves for ssRNA and dsDNA are more hyperbolic with Hill coefficients of 1.5 and 2.7, respectively. EMSA analysis

Author contributions: A.P., B.W., and S.H. designed research; A.P., C.L., B.W., M.O.-J., M.L., and S.H. performed research; A.P., C.L., B.W., M.L., T.W., and S.H. analyzed data; and A.P. and S.H. wrote the paper.

The authors declare no conflict of interest.

This article is a PNAS Direct Submission.

[1]To whom correspondence should be addressed. E-mail: hur@idi.harvard.edu.

This article contains supporting information online at www.pnas.org/lookup/suppl/doi:10.1073/pnas.1113651108/-/DCSupplemental.

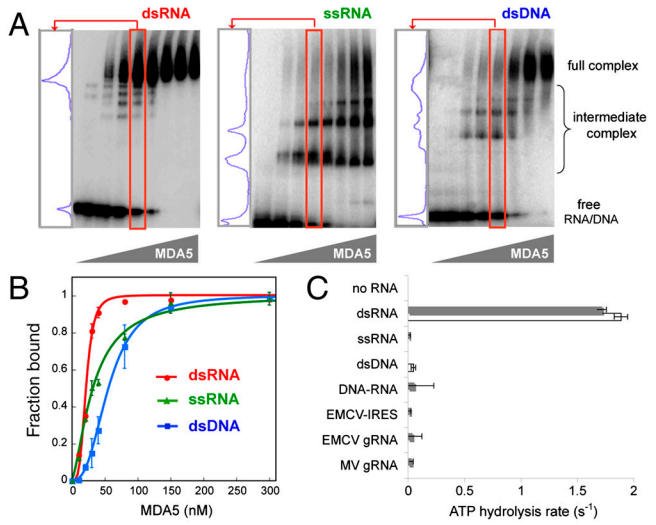

Fig. 1. Only binding of MDA5 to dsRNA is cooperative and stimulates ATP hydrolysis. (*A*) EMSA with 112 bp/nt dsRNA, ssRNA, and dsDNA. A lane in which approximately 50% of MDA5 is bound to the respective nucleic acid (red box) was chosen for each sample, and the distribution of the complexes is displayed in the left-hand panel. (*B*) The EMSA results in *A* were fit to the Hill equation to obtain dissociation constant (K_d) and Hill coefficient (Nh). Estimated K_d and Nh are 22 nM and 4.0 for dsRNA, 33 nM and 1.5 for ssRNA, and 57 nM and 2.7 for dsDNA, respectively. Plotted values are mean ± SD ($n = 2$). (*C*) ATP hydrolysis rates (mean ± SD, $n = 4$) of MDA5 (0.3 μM) free of nucleic acids, MDA5 bound to 112 bp/nt dsRNA, ssRNA, dsDNA, DNA–RNA hybrid (■ sequence 1, □ sequence 2, see Table S1), IRES (1 kb), and genomic RNA (gRNA) (~7 kb) of EMCV and MV. Equivalent mass concentration (4.8 μg/mL) was used for all nucleic acids.

of another 112 bp dsRNA with different sequence (dsRNA2, Table S1) reveals a similar bimodal distribution of RNA upon MDA5 binding and sigmoidal binding curve (Fig. S1*B*), suggesting that highly cooperative binding of MDA5 is dependent on dsRNA structure but not sequence.

Only dsRNA Stimulates ATP Hydrolysis by MDA5. We next asked whether the ATP hydrolysis activity of MDA5 is dependent on the type of bound nucleic acid. We measured the ATP hydrolysis rate of MDA5 using two sets of 112 bp/nt dsRNAs, ssRNAs, or dsDNAs derived from two different sequences (Table S1) at an equivalent nucleotide concentration (4.8 μg/mL, i.e., 71.4 nM 112 bp dsRNA). The ATP hydrolysis activity of MDA5 was strongly stimulated by dsRNAs, but not by ssRNAs or dsDNAs (Fig. 1*C*), consistent with previous observations (20). A 112 bp RNA–DNA hybrid and 7 kb genomic ssRNAs derived from two picornaviruses, encephalomyocarditis virus (EMCV) and Mengo virus (MV), which contain highly structured internal ribosome entry sites (IRES) were also unable to stimulate ATP hydrolysis (Fig. 1*C*). This result suggests that dsRNA is the only type of nucleic acid that supports MDA5 ATP hydrolysis.

MDA5 Forms Filamentous Oligomers Along the Length of dsRNA. To better understand the nature of the interaction of MDA5 with dsRNA in comparison with ssRNA and dsDNA, we visualized complexes of MDA5 with nucleic acids using negative-stain EM. We included the cross-linker reagent, bismaleimide (BMH), and ATP analogue, ADP-aluminum fluoride (ADP•AlF_4) in the sample preparation to improve complex homogeneity and stability (Fig. S2*A*). The migration of the BMH-cross-linked MDA5:dsRNA complex was identical to that observed for the native complex by EMSA.

The electron micrographs of the MDA5:dsRNA:ADP•AlF_4 complex revealed that MDA5 forms a filamentous oligomer upon binding to 112 bp dsRNA (Fig. 2*A*). Rod-like oligomers were rarely observed with ssRNA and dsDNA, (<3% of dsRNA), and were more heterogeneous in size (Fig. S2*C*). Each nucleoprotein filament of MDA5 with 112 bp dsRNA is 32–37-nm long. RNA is not directly visible in the negatively stained samples, but the agreement between the observed filament length and predicted length of 112 bp dsRNA (~33 nm, ~2.8 Å helical rise per base pair) supports the idea that the filament is arranged along the length of dsRNA. To test whether the filament extends with RNA length, we examined the complex formed with 512 bp dsRNA. Longer filaments of 150–170 nm were observed, consistent with the expected length of a 512 bp dsRNA molecule (Fig. 2*A*). Thus, dsRNA promotes MDA5 filament assembly along the length of dsRNA.

To obtain a more detailed understanding of the filament assembly, we calculated class averages of the 112 bp complex. Each filament consists of seven or eight segments (Fig. 2*B*). This result is in agreement with the number of intermediate complex bands in EMSA (Fig. 2*C*), suggesting that each segment corresponds to

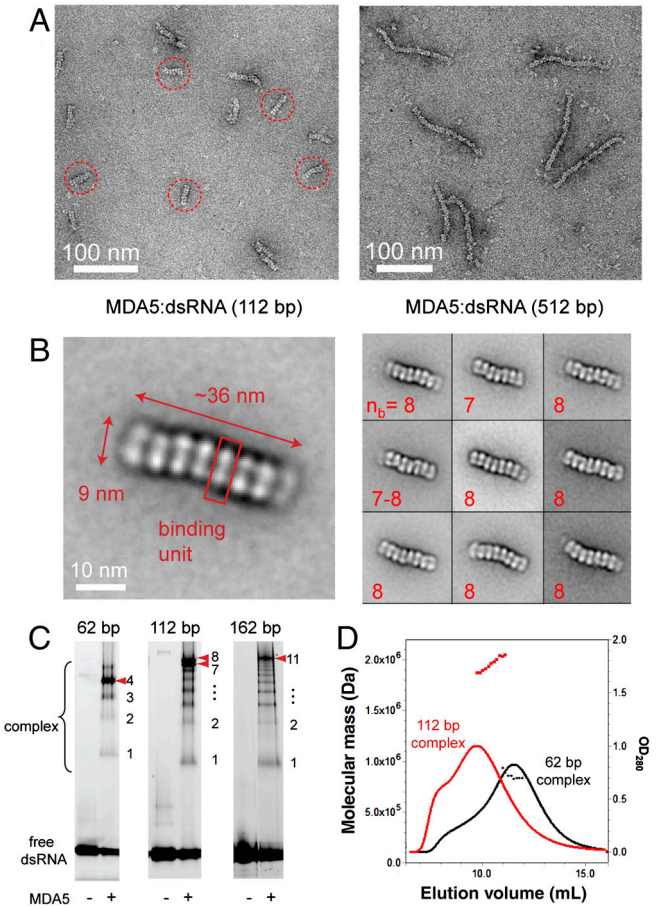

Fig. 2. MDA5 forms filamentous oligomers along the length of dsRNA. (*A*) Representative electron micrographs of negatively stained MDA5 in complex with 112 and 512 bp dsRNA in the presence of ADP•AlF_4. Representative particles used for averaging are circled in red. See Fig. S2*C* for electron micrographs of MDA5 in complex with ssRNA and dsDNA. (*B*) Representative class averages of MDA5 in complex with 112 bp dsRNA. The red box in the magnified view corresponds to a minimum binding unit of MDA5 in EMSA (*C*). The number of binding units per complex (n_b) is displayed at the bottom left for each average. (See also Fig. S2*D*.) (*C*) EMSA of 62, 112, and 162 bp dsRNAs with MDA5 (0.3 μM) visualized with SybrGold stain to enhace the intermediate complexes that are otherwise difficult to detect. Enumeration of intermediate complexes reveals that the full complex contains 4, 7–8, and 11 binding units of MDA5 for 62, 112, and 162 bp dsRNAs, respectively. (*D*) Multi-angle light scattering (–OD_{280} and ■ M_r estimation) suggests that the molecular mass of the full complexes formed on 62 and 112 bp dsRNAs are 854 (±43) kDa and 1,878 (±13) kDa, respectively.

the minimal binding unit. The tight packing of these segments along the filament is consistent with cooperative binding observed from EMSA. Each unit occupies approximately 1.3 helical turns of the RNA (15 bp), but no clear indications of helical symmetry could be detected in the averages or their Fourier transforms. Occasionally segments in the filaments slightly deviate from the central axis, causing a modest level of curvature in the filament; this curvature may result from heterogeneity in the ADP•AlF_4 occupancy or in the dimer-dimer interface. A more detailed analysis of the structure was not feasible because of the low resolution of the averages.

To determine the stoichiometry of the MDA5:dsRNA complex, we measured the molecular mass of the BMH-cross-linked filament using multiangle light scattering (MALS) (Fig. 2*D*). We found that MDA5 forms complexes of 854 kDa with 62 bp and 1,878 kDa with 112 bp dsRNA, which corresponds to 6.7 and 15.5 MDA5 monomers per RNA molecule, respectively. From EMSA, we observed approximately 4 and 7–8 complex bands for 62 and 112 bp dsRNAs, respectively (Fig. 2*C*). This result suggests that each segment in EM averages and each binding unit in EMSA represents an MDA5 dimer. The stoichiometry of one MDA5 dimer per 15 bp is also evident from two other supporting experiments involving MDA5 titration and EMSA examination of mixed populations of MDA5 with different sizes (Fig. S3). Interestingly, our MALS analysis (Fig. S1*A*) and a previous report (13) suggest that MDA5 is monomeric in solution, indicating that MDA5 dimerizes upon dsRNA binding. Although a complex of a single MDA5 monomer bound to dsRNA is often undetectable by EMSA with dsRNA longer than 62 bp, it is apparent with 15 bp dsRNA (Fig. S3*B*). This finding suggests that dimerization is cooperative only in the context of filament.

ATP Hydrolysis Occurs by Monomers of MDA5 Throughout the Filament. The unique property of dsRNA in promoting both filament assembly and ATP hydrolysis by MDA5 raised the question of whether filament formation is required for ATP hydrolysis, and whether ATP hydrolysis of an MDA5 molecule depends on its position within a filament. To address these questions, we examined ATP hydrolysis activity of MDA5 with 15, 112, and 512 bp dsRNAs. To account for the low binding affinity of MDA5 to 15 bp (K_d of 949 nM, Fig. S3*C*) and to measure the intrinsic ATP hydrolysis activity of MDA5 (instead of binding or dissociation kinetics which often dominate the steady-state reaction rate at low enzyme or substrate concentration), we measured ATP hydrolysis rates using high concentration of MDA5 (4 μM) or dsRNA (40 μg/mL, i.e., 10.7 μM MDA5 binding site) that would saturate 0.6 μg/mL dsRNA or 0.3 μM MDA5, respectively. Use of the same total base-pair (i.e., mass) concentration also ensures the same amount of MDA5 binding sites for all reactions. Note that 1 μM would occupy 3.75 μg/mL of dsRNA regardless of the RNA length (i.e., MDA5 dimer per 15 bp). We found that 15 bp dsRNA robustly stimulates MDA5 ATP hydrolysis (Fig. 3*A*) and its rate is comparable to that of 112 and 512 bp. These observations suggest that filament formation is not required for ATP hydrolysis and that an individual dimer can hydrolyze ATP with little positional preference within a filament.

To examine the interdependence of the ATP hydrolysis activity of the two MDA5 monomers in a dimeric binding unit or MDA5 molecules within a filament, we measured the ATP hydrolysis activity of heterodimers or heterofilaments formed on 15 bp or 512 bp dsRNA by a mixture of WT and catalytically inactive mutants. We used alanine mutants of K335 and D443, the two conserved residues important for ATP binding and hydrolysis (21), because these mutants do not hydrolyze ATP but retain high affinities to dsRNA (Fig. S4 *B–C*). We confirmed that WT and K335A or D443A form heterodimers and heterofilaments using EMSA (Fig. S4 *D–E*). We premixed WT and the mutants at various ratios with a fixed total MDA5 concentration, and formed a

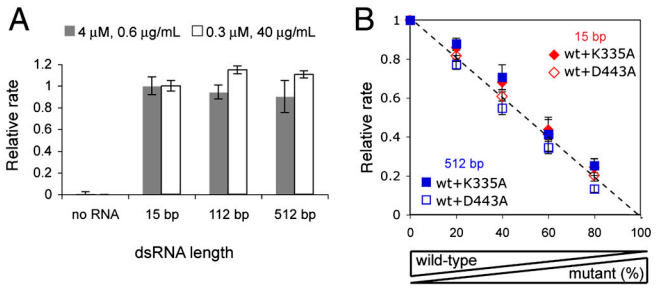

Fig. 3. Intrinsic ATP hydrolysis activity of MDA5 is independent of filament length or catalytic activity of neighboring molecules. (*A*) Relative rates of ATP hydrolysis (mean ± SD, $n = 3$) of MDA5 (4 or 0.3 μM) with and without 15, 112, and 512 bp dsRNAs (0.6 or 40 μg/mL, equivalent to 0.16 or 10.7 μM MDA5 binding site), with respect to 15 bp rates. (*B*) Relative rates of ATP hydrolysis of mixtures of WT MDA5 and K335A or D443A at indicated ratios with total MDA5 concentration fixed at 0.3 μM. The protein mixture was incubated with 40 μg/mL (10.7 μM MDA5 binding site) of 15 or 512 bp dsRNA. Rates were normalized against that with 100% WT.

complex with a 15 or 512 bp dsRNA with the same two conditions used in Fig. 3*A* (Fig. 3*B* and Fig. S4*F*). In all cases, the ATP hydrolysis rate per WT (derived from the relative rate in Fig. 3*B* and Fig. S4*F* divided by the WT concentration) remained constant. These results suggest that the intrinsic ATP hydrolysis activity of a WT subunit is unaffected by the catalytic activity of its dimeric partner or neighboring molecules within a filament.

ATP Hydrolysis by MDA5 Promotes Dissociation from dsRNA. Previous studies with several helicases suggested that ATP hydrolysis can trigger their dissociation from RNA (21, 22). To test the effect of ATP hydrolysis on the interaction between MDA5 and dsRNA, we performed a time-dependent EMSA, in which the time evolution of the level of MDA5:dsRNA complex was monitored in the presence of a protein trap, heparin, which binds MDA5 but does not stimulate ATP hydrolysis. MDA5 was preincubated with 512 bp RNA, and the reaction was initiated by adding a mixture of ATP and a 166-fold excess of heparin relative to RNA. The ability of heparin to trap MDA5 at this ratio was confirmed from EMSA in which a premixture of MDA5 with heparin prevents MDA5 binding to dsRNA (Fig. S5*C*). In the absence of ATP (Fig. 4*A*), MDA5:dsRNA complex is stable with less than 30% of conversion of total dsRNA to free dsRNA within 5 min. Similar stability was observed for both catalytic mutants, K335A and D443A, in the presence of ATP (Fig. S5*D*). This stability is in contrast to WT MDA5 with ATP where approximately 50% of dsRNA was free of MDA5 within 15 s (Fig. 4*A*). To examine whether the rapid dissociation of WT is due to hydrolysis or binding of ATP, we replaced ATP by a nonhydrolyzable ATP analogue, β,γ-methyleneadenosine 5′-triphosphate (ADPCP) in the dissociation reaction. ADPCP binds to MDA5 as evidenced by its inhibition of ATP-hydrolysis activity but does not interfere with electrophoresis which is the case for ADP•AlF_4 (Fig. S5 *A–B*). In the presence of ADPCP, approximately 50% of total dsRNA was converted to free RNA in 5 min, as opposed to 15 s for ATP (Fig. 4*A*). Thus, the ATP-dependent rapid dissociation WT MDA5 is primarily due to ATP hydrolysis.

Consistent with the above result, a single-round ATP hydrolysis assay also revealed similar dissociation kinetics during ATP hydrolysis. We monitored ATP hydrolysis by MDA5 in complex with 512 bp dsRNA in the presence and absence of heparin. The initial rates for both reactions were comparable. However, the rate with heparin declined to a halt within 1 min, whereas the rate without heparin remained constant over 3 min (Fig. 4*B*). The overlapping time interval for ATP hydrolysis and dissociation kinetics suggests that the rapid decrease in the ATP hydrolysis rate in the heparin reaction is due to MDA5 dissociation from dsRNA.

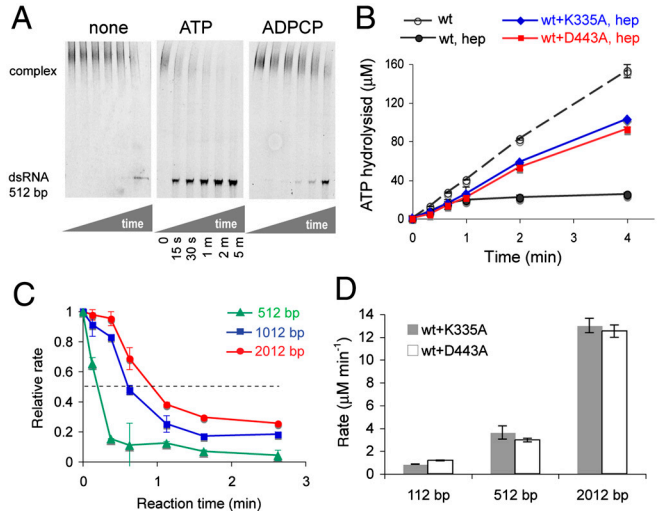

Fig. 4. Disassembly of MDA5 filament is both ATP and RNA length-dependent. (*A*) Time-dependent EMSA monitoring of MDA5:RNA complex dissociation. The reaction was initiated by adding a mixture of 2 mM ATP (or ADPCP or no ligand) and 200 μg/mL heparin to MDA5 (1.35 μM) in complex with 512 bp dsRNA (1.2 μg/mL, 0.32 μM MDA5 binding site), quenched on ice at indicated time points and analyzed on native gel. (*B*) Single-round ATP hydrolysis kinetics (mean ± SD, $n = 3$) of WT MDA5 (0.1 μM) with and without K335A or D443A (0.1 μM) bound to 512 bp dsRNA (1.2 μg/mL) with and without heparin (hep, 200 μg/mL). (*C*) Time evolution of the ATP hydrolysis rate derived from the single-round kinetics (Fig. S5*F*) of WT MDA5 (0.2 μM) bound to 512, 1,012, and 2,012 bp dsRNAs (1.2 μg/mL) using the finite difference method. The rates were normalized against the initial rate during the first 15 s. (*D*) Single-round ATP hydrolysis rate of WT MDA5 (0.1 μM) with K335A or D443A (0.1 μM) bound to 512, 1,012, and 2,012 bp dsRNAs (1.2 μg/mL) in the presence of heparin (200 μg/mL) during 4–10 min. No ATP hydrolysis was observed without the mutants during this time period.

Catalytic Mutants Inhibit ATP-Dependent Dissociation of Wild-Type MDA5 from dsRNA. To test interdependence of dissociation among individual MDA5 molecules within a filament, we examined the effect of K335A and D443A on ATP-dependent dissociation of WT MDA5. We first mixed WT MDA5 with the mutants, and performed the single round kinetic assays using 512 bp dsRNA. Unlike the reaction of WT alone with heparin, which stops within 1 min, the reactions with K335A and D443A progressed over 4 min at a rate 70% of that of WT alone without heparin. This result suggests that 70% of WT MDA5 remained bound to dsRNA over 4 min in the presence of K335A or D443A. This interpretation is supported by a pull-down assay with biotinylated RNA, which showed that WT copurifies with dsRNA after 3 min incubation with ADPCP but not with ATP (Fig. S5*E*). Addition of K335A/D443A to the ATP reaction restores the level of WT copurified with dsRNA. Thus, the catalytic mutants stabilize the WT complex and dissociation of individual MDA5 molecules is interdependent.

ATP-Driven MDA5 Dissociation is Filament Length-Dependent. We next asked whether ATP-dependent MDA5 dissociation depends on the length of the filament. If every ATP hydrolysis event were equally capable of dissociating an individual MDA5 molecule from both filament interiors and ends, the dissociation rate would be independent of the initial filament length. This prediction would also be true if a filament disassembles cooperatively, either as an entire filament or in smaller fragments, when a fraction of MDA5 monomers hydrolyzing ATP at a time reaches a certain threshold that is independent of filament length (i.e., linearly increasing stability). Alternatively, if filament disassembly occurs from an end as individual monomers or dimers, or disassembles cooperatively with a higher threshold for longer filaments (i.e., nonlinearly increasing stability), MDA5 would dissociate more slowly from longer dsRNA. We compared the dissociation rate of WT MDA5 using the single-round kinetic assay with 512, 1,012, and 2,012 bp dsRNAs. The time derivative of the single-round kinetics (Fig. S5*F*) showed a more rapid reduction of the ATP hydrolysis rate for shorter dsRNAs with half-lives of 0.2, 0.6, and 1.3 min for 512, 1,012, and 2,012 bp dsRNAs, respectively (Fig. 4*C*). The more rapid decline in the ATP hydrolysis rate with shorter dsRNAs suggests a more rapid dissociation of MDA5 from shorter dsRNAs, which is inconsistent with models in which MDA5 dissociates from the filament interiors or cooperatively with its threshold independent of filament length.

To further validate the length-dependent dissociation mechanisms, we utilized the K335A/D443A mutants to stall the dissociation reaction, and compared the level of WT that remained bound to dsRNAs of different lengths using the single-round kinetic assay. WT was premixed with an equal amount of K335A/D443A, and complexes were formed with dsRNAs of 112, 512, and 2,012 bp at the equivalent total base-pair concentration. To ensure equivalent binding of WT to dsRNA at the beginning of the reaction, we used 0.2 μM MDA5, which is 10-fold higher than the value of K_d for 112 bp (Fig. 1*B*). We measured ATP hydrolysis progression between 4 and 10 min during which no ATP hydrolysis was observed for the WT alone reaction. In the presence of K335A or D443A, however, ATP hydrolysis continued during this time frame and the rate correlated with dsRNA length; the fold increase in the rate from 112 to 512 bp and 2,012 bp is 4.3 and 15.4 for K335A and 2.5 and 10.7 for D443A, in comparison to a 4.6- and 18-fold increase in length (Fig. 4*D*). In principle, if disassembly occurs only from a filament end, the rate ratios would be equal to or greater than the length ratios. The closely matching of rate and length ratios suggests that end disassembly could be the primary mechanism with some level of interior dissociation, or that the filament disassembles cooperatively with nonlinearly increasing stability with filament length.

A Partial Loss-of-Function Mutant, I923V, Exhibits Impaired Filament Assembly and Reduced Kinetic Stability. A partial loss-of-function SNP variant I923V (Fig. 5*A*), which has been associated with a reduced risk for type 1 diabetes, was reported to have reduced signaling activity but retain similar affinity to a dsRNA mimic, poly I:C, as WT MDA5 (23, 24). We asked whether the reduced signaling by I923V is due to impaired filament assembly and stability. We found that I923V binds to 112 bp dsRNA with similar affinity but with reduced cooperativity (K_d of 18 nM vs. 22 nM, Hill coefficient of 1.9 vs. 4.0) (Fig. 5*B*).

Consistent with low cooperative binding, EM revealed that I923V is less efficient in filament formation with 112 bp dsRNA (Fig. 5*C*). The class averages revealed that the overall RNA binding modes of I923V and WT are similar, but the I923V complex contains 4–7 dimers rather than the 7–8 dimers seen in the WT complex. The histogram analysis of filament length distribution also indicates that 45% of the WT complexes are approximately 36-nm long, whereas only 15% of the I923V complexes are 36 nm and 60% are 27–31.5 nm (Fig. 5*D*). Consistent with this finding, the molecular mass of the I923V:112 bp dsRNA complex estimated from MALS is 209 kDa (~1 dimer) less than that of the WT complex (Fig. S6*C*).

We next examined the kinetic stability of I923V using the single-round ATP hydrolysis assay. Both WT and I923V were complexed with 2,012 bp dsRNA, and the progression of the ATP hydrolysis reaction in the presence of heparin was monitored (Fig. 5*E*). Although both reactions initiated with similar efficiencies, the I923V reaction reached a plateau faster than the WT reaction, resulting in a lower level of ATP hydrolyzed during the single-binding event. Rate analysis suggests that I923V dissociates from dsRNA approximately four times more rapidly than WT (Fig. 5*F*). This finding suggests that I923V has a reduced kinetic stability compared with WT, and supports our hypothesis

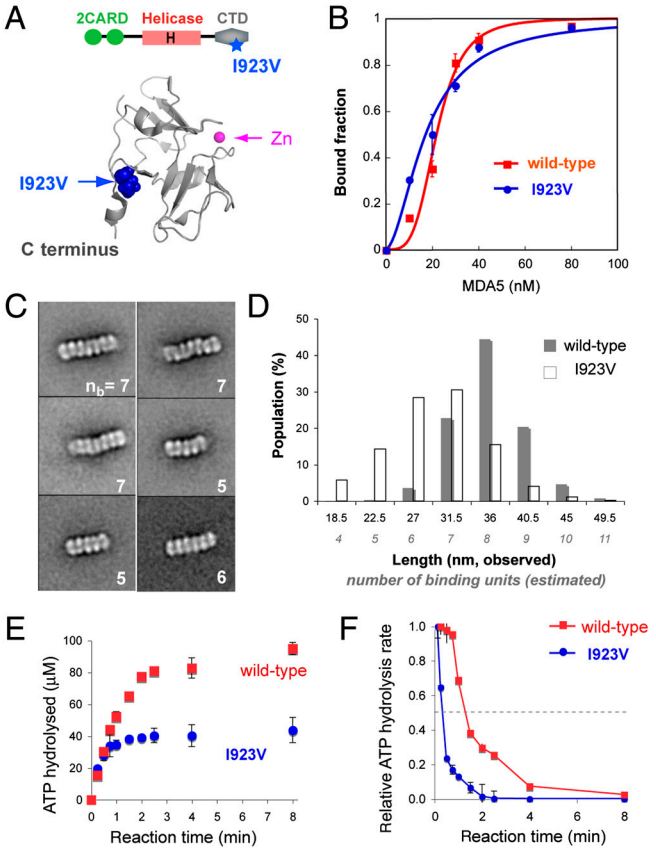

Fig. 5. SNP I923V forms shorter filaments and exhibits decreased kinetic stability. (*A*) Cartoon representation of MDA5 CTD [Protein Data Bank (PDB) ID code 2RQB]. Residue I923, distal to the Zn coordination site but proximal to the C terminus, is partially solvent-exposed. (*B*) EMSA binding curves (mean ± SD, $n = 2$) of WT and I923V MDA5 with 112 bp dsRNA. (*C*) Representative class averages of I923V in complex with 112 bp dsRNA. The number of binding units (n_b) present for each complex is displayed at the bottom right. See also Fig. S6*D*. (*D*) Histogram of the length distribution of complexes formed by WT and I923V with 112 bp dsRNA. Each length represents the median value of each interval. The number of binding units per complex was estimated from the complex length. (*E*) Single-round ATP hydrolysis kinetics (mean ± SD, $n = 3$) of WT and I923V (0.2 μM) bound to 2,012 bp dsRNAs (1.2 μg/mL) in the presence of heparin (200 μg/mL). (*F*) Time evolution of the ATP hydrolysis rate derived from *E* using the finite difference method. Rates were normalized against the initial rate during the first 15 s.

that extended filament formation is important for maintaining kinetic stability of the MDA5:dsRNA complex.

Discussion

The molecular mechanism for recognition of long (>1–2 kb) viral dsRNA by MDA5 remains poorly understood, and our limited understanding has been largely inferred from knowledge of a paralogous receptor, RIG-I, despite its divergent RNA and viral specificity. We report here the previously uncharacterized architecture of a filamentous assembly of MDA5 on dsRNA, and its dynamic ATP-dependent disassembly to provide a mechanism of how MDA5 both recognizes dsRNA and auto-regulates its antiviral signaling activity in a length-dependent manner.

We demonstrate here that binding affinity alone is insufficient to confer dsRNA specificity to MDA5 with high-affinity binding observed for multiple types of nucleic acids. Despite low stringency nucleic acid discrimination on the basis of affinity, MDA5 is able to distinguish between dsRNA and other types of nucleic acids through cooperative filamentous assembly along the length of dsRNA. Analogous filament structures have been observed with RecA which forms filamentous oligomers along DNA and promotes strand exchange during homologous recombination (25). MDA5 is structurally related to RecA in that its central helicase domain consists of two RecA-like subdomains. However, unlike the RecA filament whose formation requires ATP binding (26), MDA5 filament formation does not require ATP or its analogues (Figs. S2*A* and S5*A*). We speculate that the C-terminal domain (CTD) of MDA5, which is absent in RecA, plays an important role in the cooperative assembly process of the filament. A partial loss-of-function mutation, I923V, within the CTD lowers both the cooperativity and the extent of filament assembly without affecting the dsRNA affinity of MDA5 (Fig. 5). In addition, replacement of the MDA5 CTD by the RIG-I CTD abolishes the cooperativity while retaining high-affinity interaction with dsRNA (Fig. S6*E*). Filament formation was recently proposed for RIG-I based on atomic force microscopy (16); however, we did not observe either filament formation of RIG-I by EM or cooperative binding by EMSA (Fig. S2*B*).

We demonstrated that the MDA5:dsRNA filament is a highly dynamic structure, the stability of which is tightly regulated by ATP hydrolysis. Using quantitative single- and multiround kinetic analysis and catalytic mutant interference studies, we provide evidence supporting that ATP hydrolysis occurs throughout the filament with little coordination between neighboring MDA5 molecules (Fig. 3). ATP hydrolysis-driven MDA5 dissociation, however, occurs in a coordinated manner as evidenced by a markedly increased stability of a filament upon incorporation of catalytically inactive mutants (Fig. 4*B*). This coordinated dissociation occurs at a rate inversely proportional to the filament length (Fig. 4*C*), suggesting that not every ATP hydrolysis event leads to MDA5 dissociation. We propose two mechanisms to explain this length-dependent dissociation. First, MDA5 may dissociate from dsRNA as monomers or dimer pairs from filament extremities. This end dissociation could be because MDA5 molecules in the filament ends are less stable than those in the interiors due to the lack of stabilizing contacts with neighboring molecules. Based on this end-disassembly model, the positive effect of the catalytic mutants on the filament stability could be explained by the mutants capping the filament ends and preventing progression of filament disassembly. Second, MDA5 may cooperatively dissociate from dsRNA as an entire filament or smaller fragments whose stability increases nonlinearly with filament length. In this model, the catalytic mutants may increase filament stability by increasing the threshold required for filament disassembly by ATP hydrolysis.

The dual and seemingly opposing roles of ATP hydrolysis as both a consequence of filament formation (or dsRNA binding) and as a trigger for filament disassembly is reminiscent of the roles of nucleotide hydrolysis in other filamentous proteins, such as RecA, actin, and tubulin. These proteins utilize either repetitive or single-round of nucleotide hydrolysis as a counterbalance between filament growth and turnover (25, 27). Competition between the filament assembly and disassembly processes was also evident for MDA5 in EMSA during the ATP hydrolysis steady state, which revealed reduced apparent affinity in comparison without ATP (Fig. S5*A*). Although comprehensive understanding of the MDA5 filament dynamics would require more detailed knowledge on both assembly and disassembly processes, the observed length-dependent dissociation provides a basis for how MDA5 could self-regulate its interaction with dsRNA and thus antiviral signaling potential according to the underlying dsRNA length. This notion is in agreement with the known requirement of long (>1–2 kb) dsRNA to efficiently elicit interferon signaling activity of MDA5 in the cell (8). Thus, our observations suggest a previously unrecognized role of ATP hydrolysis in autoregulation of MDA5 filament growth and turnover.

The highly cooperative MDA5 filament formation raises intriguing possibilities for other antiviral functions of MDA5. As many receptors in the immune system cluster for effective signal

transmission (17, 18), clustering of MDA5 on dsRNA may facilitate recruitment of MAVS or subsequent oligomerization of MAVS, which itself was recently shown to form prion-like fibrillar structures during antiviral signaling (10). It has been proposed that recruitment of MAVS by MDA5 depends on a conformational change of MDA5 induced by ATP hydrolysis (1, 10). It would be interesting to test whether ATP hydrolysis by individual MDA5 molecules within a filament recruits MAVS and promote their oligomerization through induced proximity. In addition, MDA5 filament formation may also perform a unique antiviral effector function by limiting access of viral proteins to RNAs, thereby interfering with viral replication or packaging. Interestingly, a recent study identified MDA5, along with RIG-I, as one of the most broadly acting antiviral effectors (28). Our present studies provide a basis for future investigations on more detailed mechanisms and functions of MDA5 in antiviral defense.

Experimental Procedures

Electron Microscopy. Methods for protein and RNA preparation are described in *SI Text*. MDA5 was incubated with a 20:1 molar ratio of MDA5 to 112 bp dsRNA (ssRNA or dsDNA) in 20 mM Hepes, pH 7.0, 150 mM NaCl, 5 mM ADP•AlF_4, and cross-linked using 0.4 mM BMH at room temperature (RT) for 30 min. Negatively stained specimens were prepared as described in ref. 29. Images were collected with a Tecnai T12 electron microscope (FEI) and processed using the SPIDER software package (see *SI Text*).

Multiangle Light Scattering. The absolute molecular mass of the complexes formed by WT MDA5 or I923V with dsRNA was determined using a Superose 6 10/300 column (GE) attached to a miniDAWN TREOS detector (Wyatt Technology) in 20 mM Hepes, pH 7.0, 75 mM NaCl. MDA5:dsRNA complexes were prepared as for EM.

Electrophoretic Mobility Shift Assay. EMSA was performed using 5′-^{32}P-, 3′-fluorescein- or Cy3-labeled RNAs. Unless mentioned otherwise, 0.2 nM of ^{32}P-labeled RNA was mixed with the indicated amount of MDA5 in buffer A (20 mM Hepes, pH 7.5, 150 mM NaCl, 1.5 mM $MgCl_2$, and 2 mM DTT) with 2 mM ADPCP. The mixture was incubated at RT for 10 min and were analyzed on BisTris native gels (Life). For time-dependent EMSA, reactions were incubated at 37 °C for indicated time period.

ATP Hydrolysis Assay. The ATP hydrolysis rate (initial velocity) was determined using Green Reagent (Enzo) (30). Unless mentioned otherwise, MDA5 was preincubated with RNA in buffer A at 37 °C, and the reaction was initiated by addition of 2 mM ATP. For single-round kinetic assays, a mixture of 200 μg/mL heparin and 2 mM ATP was added to the reaction. For initial velocity measurement, aliquots were withdrawn at five time points between 15 s and 30 min, and were quenched with 50 mM EDTA on ice. The Green Reagent was added to the quenched reaction at a ratio of 9:1, and OD_{650} was measured using a Synergy2 plate reader (BioTek).

ACKNOWLEDGMENTS. We thank S.C. Harrison for discussions; A. Palmenberg for encephalomyocarditis virus and Mengo virus cDNA; M. Eck for sharing the multiangle light scattering instrument. A.P. and B.W. acknowledge postdoctoral fellowships from GlaxoSmithKline. T.W. is an Investigator in the Howard Hughes Medical Institute. S.H. is the recipient of a New Investigator Award (Massachusetts Life Sciences Center) and a Pew Scholarship.

1. Wilkins C, Gale M, Jr. (2010) Recognition of viruses by cytoplasmic sensors. *Curr Opin Immunol* 22:41–47.
2. Rehwinkel J, Reis e Sousa C (2010) RIGorous detection: Exposing virus through RNA sensing. *Science* 327:284–286.
3. Loo MY, et al. (2008) Distinct RIG-I and MDA5 signaling by RNA viruses in innate immunity. *J Virol* 82:335–345.
4. Kato H, et al. (2006) Differential roles of MDA5 and RIG-I helicases in the recognition of RNA viruses. *Nature* 441:101–105.
5. Baum A, Sachidanandam R, Garcia-Sastre A (2010) Preference of RIG-I for short viral RNA molecules in infected cells revealed by next-generation sequencing. *Proc Natl Acad Sci USA* 107:16303–16308 and erratum (2010) 108:3092.
6. Schlee M, et al. (2009) Recognition of 5′ triphosphate by RIG-I helicase requires short blunt double-stranded RNA as contained in panhandle of negative-strand virus. *Immunity* 31:25–34.
7. McCartney SA, et al. (2008) MDA-5 recognition of a murine norovirus. *PLoS Pathog* 4: e1000108.
8. Kato H, et al. (2008) Length-dependent recognition of double-stranded ribonucleic acids by retinoic acid-inducible gene-I and melanoma differentiation-associated gene 5. *J Exp Med* 205:1601–1610.
9. Zeng W, et al. (2010) Reconstitution of the RIG-I pathway reveals a signaling role of unanchored polyubiquitin chains in innate immunity. *Cell* 141:315–330.
10. Hou F, et al. (2011) MAVS forms functional prion-like aggregates to activate and propagate antiviral innate immune response. *Cell* 146:1–14.
11. Bamming D, Horvath CM (2009) Regulation of signal transduction by enzymatically inactive antiviral RNA helicase proteins MDA5, RIG-I, and LGP2. *J Biol Chem* 284:9700–9712.
12. Yoneyama M, et al. (2004) The RNA helicase RIG-I has an essential function in double-stranded RNA-induced innate antiviral responses. *Nat Immunol* 5:730–737.
13. Cui S, et al. (2008) The C-terminal regulatory domain is the RNA 5′-triphosphate sensor of RIG-I. *Mol Cell* 29:169–179.
14. Andrejeva J, et al. (2004) The V proteins of paramyxoviruses bind the IFN-inducible RNA helicase, mda-5, and inhibit its activation of the IFN_{-1} promoter. *Proc Natl Acad Sci USA* 101:17264–17269.
15. Saito THR, et al. (2007) Regulation of innate antiviral defenses through a shared repressor domain in RIG-I and LGP2. *Proc Natl Acad Sci USA* 104:582–587.
16. Binder M, et al. (2011) Molecular mechanism of signal perception and integration by the innate immune sensor retinoic acid inducible gene-I. *J Biol Chem*, 286 pp:27278–27287.
17. Davis BK, Wen H, Ting JP-Y (2011) The inflammasome NLRs in immunity, inflammation, and associated diseases. *Annu Rev Immunol* 29:707–735.
18. Sigalov AB (2010) The SCHOOL of nature. *Self Nonself* 1:4–39.
19. Ablasser A, et al. (2009) RIG-I-dependent sensing of poly (dA:dT) through the induction of an RNA polymerase III-transcribed RNA intermediate. *Nat Immunol* 10:1065–1072.
20. Kang DC, et al. (2002) mda-5: An interferon-inducible putative RNA helicase with double-stranded RNA-dependent ATPase activity and melanoma growth-suppressive properties. *Proc Natl Acad Sci USA* 99:637–642.
21. Linder P, Jankowsky E (2011) From unwinding to clamping- the DEAD box RNA helicase family. *Nat Rev Mol Cell Biol* 12:505–516.
22. Cordin O, Banroques J, Tanner NK, Linder P (2006) The DEAD-box protein family of RNA helicases. *Gene* 17–37.
23. Nejentsev S, Walker N, Riches D, Egholm M, Todd JA (2009) Rare variants of IFIH1, a gene implicated in antiviral responses, protect against type 1 diabetes. *Science* 324:387–389.
24. Chistiakov DA, Voronova NV, Savost'Anov KV, Turakulov RI (2010) Loss-of-function mutations E6 27X and I923V of IFIH1 are associated with lower poly(I:C)-induced $interferon_{-1}$ production in peripheral blood mononuclear cells of type 1 diabetes patients. *Hum Immunol* 71:1128–1134.
25. Cox MM (2007) Motoring along with the bacterial RecA protein. *Nat Rev Mol Cell Biol* 8:127–138.
26. Chen Z, Yang H, Pavletich NP (2008) Mechanism of homologous recombination from the RecA-ssDNA/dsDNA structures. *Nature* 453:489–494.
27. Kueh HY, Michison TJ (2009) Structural plasticity in actin and tubulin polymer dynamics. *Science* 325:960–963.
28. Schoggins JW, et al. (2011) A diverse range of gene products are effectors of the type I interferon antiviral response. *Nature* 472:481–485.
29. Ohi M, Li Y, Cheng Y, Walz T (2004) Negative staining and image classification—powerful tools in modern electron microscopy. *Biol Proced Online* 6:23–34.
30. Martin B, Pallen CJ, Wang JH, Graves DJ (1985) Use of fluorinated tyrosine phosphates to probe the substrate specificity of the low molecular weight phosphatase activity of calcineurin. *J Biol Chem* 260:14932–14937.